Application of fractal models to delineate mineralized zones in the Pulang porphyry copper deposit,Yunnan, Southwest China

Xiaochen Wang[a], Qinglin Xia[a,b,*], Tongfei Li[a], Shuai Leng[a], Yanling Li[a], Li Kang[a], Zhijun Chen[a], Lianrong Wu[c]

[a] Faculty of Earth Resources, China University of Geosciences, Wuhan 430074, China

[b]Collaborative Innovation Center for Exploration of Strategic Mineral Resources, Wuhan 430074, China

[c]Yunnan Diqing Nonferrous MetalCo., Ltd., Shangri-La674400, China

Abstract

The purpose of this study is to delineate various mineralized zones and the barren host rocks based on the surface and subsurface lithogeochemical data using the concentration–volume (C–V) and power spectrum–volume (S–V) fractal models in the Pulang porphyry copper deposit, southwest China. Results obtained by the concentration–volume model depict four geochemical zones defined by Cu thresholds of 0.25%, 1.38% and 1.88%, which represent non-mineralized wall rocks (Cu<0.25%), weakly mineralized zones (0.25%–1.38%), moderately mineralized zones (1.38%–1.88%), and highly mineralized zones (Cu>1.88%). S–V model is used by performing 3D fast Fourier transformation on assay data in the frequency domain. The S–V method reveals three mineralized zones characterized by Cu threshold values of 0.23% and 1.33%. The zones of <0.23% Cu represent barren host rocks and zones of 0.23%-1.33% Cu represent the hypogene zones and zones >1.33% Cu represent supergene enrichment zones. Both the multifractal models show that high grade mineralization is located at the center and southern parts of Pulang deposit. The results are compared with the alteration and mineralogical models resulted from the 3D geological model using the logratio matrix method. The results show that the S–V model gives better results to identify highly mineralized zones in the deposit. However, the results of C–V method for moderately and weakly grade mineralization zones are more accurate than the zones obtained from S–V method.

Keywords: Fractal; Concentration–volume model (C–V); Power spectrum–volume model (S–V); Mineralized zone; the Pulang porphyry copper deposit

1. Introduction

The delineation and recognization of various mineralized zones and non–mineralized wall rocks are the main goal in the mineral exploration work. Investigation of ore mineralogy and paragenetic sequence provides useful data on ore-forming processes in deposits, because the typical characteristics of various types of ore deposits are reflected by their mineral assemblages (Craig and Vaughan, 1994; White and Hedenquist, 1995). Common methods are usually based on mineralography, petrography and alteration minerals assemblages to delineate various mineralized zones in porphyry deposits (Beane, 1982; Schwartz, 1947; Sillitoe, 1997; Berger et al., 2008). Lowell (1968) firstly proposed a conceptual model of lateral and vertical variations in mineralogy within alteration zones. Some similar models were developed related to potassic alteration usually situated in the center and deep parts of porphyry ore deposits based on this model (Sillitoe and Gappe, 1984; Cox and Singer, 1986; Melfos et al., 2002). There are also other methods such as stable isotope studies and fluid inclusion to outline various mineralization phases based on thermometric and isotope element parameters along with other geological particulars (Boyce et al., 2007; Faure et al., 2002; Wilson et al., 2007). The drillhole data with a logging information containing mineralographical information, host rock changes and alteration is helpful to delineate the mineralization zones. Different geological interpretations could be presented for detecting zone boundaries, which may also lead to different results because the elemental grade distribution may not be taken into consideration.

Non-Euclidian fractal geometry is an significant branch of non-linear mathematical sciences. It is utilized in various research fields of geosciences since the 1980s (Mandelbrot, 1983). The relationships between geology, geochemistry and mineralogical settings with spatial information can be researched by the methods based on fractal geometry (Afzal et al., 2011; Carranza, 2008, 2009). Bolviken et al.

(1992) and Cheng et al. (1994) have shown that geochemical patterns of various elements have fractal dimensions. The concentration–area (C–A) fractal model was proposed by Cheng et al. (1994) to recognize geochemical anomalies from backgrounds and calculate elemental thresholds of different geochemical data. Furthermore, there are many other fractal models proposed and applied in geochemical exploration work including number–size (N–S) fractal model proposed by Mandelbrot (1983) and Agterberg (1995), power spectrum–area (S–A) fractal model proposed by Cheng et al.(1999), concentration–distance (C–D) fractal model proposed by Li et al. (2003), concentration–volume (C–V) fractal model proposed by Afzal et al. (2011) and power spectrum–volume (S–V) fractal model proposed by Afzal et al. (2012).

Methods of fractal analysis also serve to illustrate relationships of geological, geochemical and mineralogical settings with spatial information derived from analysis of mineral deposit occurrence data (Carranza, 2008, 2009, 2010; Carranza et al., 2009; Goncalves et al., 2001; Wang et al., 2011; Zuo et al., 2009). Different geochemical processes could be described based on differences within fractal dimensions obtained from research of relevant geochemical data. Afzal et al.(2011) considered that the log–log plots obtained by fractal methods are useful tools to delineate different geological populations of geochemical data and the thresholds could be determined as some break points in those plots.

The application of fractal models to delineate various grade mineralization zones was dependent on the relationships between metal grades and volumes (Afzal et al., 2011; Cheng, 2007; Sim et al., 1999; Agterberg et al., 1993; Turcotte, 1986). The concentration–volume (C–V) and power spectrum–volume (S–V) fractal models were proposed by Afzal et al. (2011, 2012) to delineate various grade mineralization zones. We utilized C–V and S–V fractal models to delineate various mineralized zones and barren host rocks in the Pulang copper deposit in this paper.

2. Fractal models

2.1. Concentration–volume fractal model

Afzal et al.(2011) proposed concentration–volume (C-V) fractal model based on the same idea as the concentration–area (C-A) model (Cheng et al., 1994) to analysis the relationship between the concentration of ore elements and accumulative volume with concentration greater than or equal to the presented value (Afzal et al., 2011; Sadeghi et al., 2012; Soltani et al.,2014; Zuo et al., 2016; Sun and Liu, 2014; Wang, G. et al., 2012). It could be shown as:

$$V(\rho\leq\upsilon)\propto\rho^{-a_1};\ V(\rho\geq\upsilon)\propto\rho^{-a_2} \qquad (1)$$

$V(\rho\geq\upsilon)$ and $V(\rho\leq\upsilon)$ represent those occupied volumes with concentrations above or equal to and less than or equal to the contour value υ; υ indicates the threshold value of a zone; a_1 and a_2 are the characteristic indexes. Thresholds obtained by this method indicate the boundaries between different grade mineralization zones and barren host rocks of ore deposits. The drillhole data of elemental concentration values were interpolated by using geostatistical estimation to compute $V(\rho\geq\upsilon)$ and $V(\rho\leq\upsilon)$, which are the volume values enclosed by a contour level ρ in a 3D model.

2.2. Power spectrum–volume fractal model

Different geochemical patterns in the spatial domain could be seen as layered signals of various frequencies. Cheng et al. (1999) proposed the power spectrum–area (S-A) fractal model to recognize geochemical anomalies from backgrounds utilizing the method of spectrum analysis in frequency domain according to this argument. This model is combined with concentration–area (C-A) model (Cheng et al. 1994). It offers an useful tool to determine an optimum threshold value between various patterns based on the scaling property.

Afzal et al.(2012) proposed the power spectrum–volume (S–V) fractal model to delineate different grade mineralization zones based on the same idea as the S–A model proposed by Cheng et al.(1999). S–V method was utilized in frequency domain. And it was performed by applying the fast Fourier transformation for assay data. The straight lines obtained by log–log plots indicate the relationships between power spectrums and relevant volumes of ore elements. They were utilized to recognize the hypogene zones and supergene enrichment zones from barren host rocks and leached zone of the deposit. The recognization of various mineralization zones is on the basis of the power–law relationships between power spectrums and occupied volumes. The formula is as follows:

$$V(\geq S) \propto S^{-2/\beta} \quad (2)$$

Where, the power–law relationships between power spectrums (S=−||F(Wx, Wy, Wz)||) and occupied volumes with power spectrums greater than or equal to S can be indicated by this form; F represents the fast Fourier transformation of the measurement μ(x, y, z); Wx, Wy and Wz respectively indicate wave numbers or angular frequencies in X, Y and Z axes directions on a 3D model. The range of index β is $0<\beta\leq 2$ or $1\leq 2/\beta$ with the special case of $\beta=2$ or $2/\beta=1$ corresponding to non-fractal or monofractal and $1<2/\beta$ to multifractals (Cheng, 2006).

By using the method of geostatistical estimation, drill hole data of elemental concentration values were interpolated to construct the block model with ore element distribution. The power spectrum values can be obtained by using 3D fast Fourier transformation for ore element grades. The logarithm of all power spectrum values and accumulative volume values were calculated. And the log-log plot between power spectrums and volumes was drawed according to previous counted values. Then the filters were constructed on the basis of threshold values obtained by the log-log plot of S-V. Finally, the power spectrums were converted back to the space domain by utilizing inverse fast Fourier transformation.

3. The geological setting of Pulang copper deposit

The Pulang porphyry copper deposit is situated in the southern end of the Yidun continental arc, southwest China (Fig. 1). The continental arc was produced due to the westward subduction of Garze–Litang oceanic crust (Deng et al., 2014b, 2015; Wang et al., 2014). The Pulang ore deposit, one of the largest porphyry copper deposits in China (Deng et al., 2012, 2014a; Mao et al., 2012, 2014), is characterized by typical porphyry-type alteration zone. And Leng et al. (2012) and Li et al.(2011, 2013) have systematically researched the detailed geological characteristics of Pulang deposit, such as the representative alteration types and their zonation, the geometry of orebody, metallogenic time and the geodynamic settings of this deposit. The Pulang deposit consists of five ore–bearing porphyries. They cover an area of about 9 km^2, and the explored ore tonnage of Cu is estimated to be 6.50 Mt (Liu et al., 2013).

The outcrop strata of Pulang deposit are dominated by Upper Triassic Tumugou Formation clastic rocks and andesite, and Quaternary sediments (Fig.1c). The Triassic porphyry intrusions mainly comprise quartz monzonite porphyry, quartz diorite porphyry, quartz diorite porphyrite and granodiorite porphyry. The Tumugou Formation strata was intruded by the quartz diorite porphyry with an age of 219.6 ± 3.5 Ma (Zircon U–Pb dating) (Pang et al., 2009). Then quartz monzonite porphyry with an age of 212.8 ± 1.9 Ma and granodiorite porphyry with an age of 206.3 ± 0.7 Ma (Zircon U–Pb dating) (Liu et al., 2013) crosscut quartz diorite porphyry, respectively. The quartz monzonite porphyry is considered to be associated with mineralization because its age is similar with the molybdenite Re–Os isochron age of 213 ± 3.8 Ma from orebody (Zeng et al., 2004). Moreover, the Cu concentrations of quartz monzonite porphyry are higher than the other porphyries.

<Fig. 1 inserts here>

The porphyry-type alteration zones transit upward and outward from early potassium–silicate, through quartz–sericite to propylitization from the core of the quartz monzonite porphyry (Fig. 4). Most wall rocks near the porphyries were changed into hornfels. Systematic drilling has demonstrated that the potassium–silicate and quartz–sericite zones host the main orebodies. And they constitute the core of mineralized zones. And the weak mineralization appear in the propylitic zones and hornfels surrounding the core. The orebodies occur as veins within the propylitic zones and hornfels. Major rock types in the deposit are quartz monzonite porphyry, quartz diorite porphyrite, granite diorite porphyry, quartz diorite porphyry and hornfels (Fig. 2). Metallic minerals mainly include chalcopyrite, pyrite and some molybdenite and pyrrhotite (Fig. 3).

<Fig. 2 inserts here>

<Fig. 3 inserts here>

<Fig. 4 inserts here>

4. Fractal modeling

Based on the geological data of this deposit, such as the collar coordinates, azimuth, dip, mineralogy and lithology recorded from 130 drillholes, 20492 lithogeochemical samples have been collected at 2 m intervals. The laboratory of the 3rd Geological Team of the Yunnan Bureau of Geology and Mineral Resources utilized the iodine–fluorine and oscillo-polarographic method to analyze the concentrations of Cu and associated paragenetic elements and its analytical uncertainty is less than 7% (Yunnan Diqing Nonferrous Metal Co. Ltd., 2009). Only Cu concentrations were researched in this study. The distribution of Cu concentrations is log-normal (Fig. 5). The experimental semi–variogram of Cu data of Pulang deposit indicates a range and nugget effect of 320.0m and 0.25, seperately (Fig. 6). The spherical model is fitted in regard to the experimental semi–variogram. The 3D model of Cu concentrations distribution of Pulang deposit was produced with ordinary kriging method using the Geovia Surpac software on the basis of the semi–variogram and anisotropic ellipsoid. Fundamentally, the accuracy of the interpolation results mainly depends on whether the interpolation model could well fit the spatial distribution characteristics of the deposit. Ordinary kriging was used because it is compatible with a stationary model; it only involves a variogram, and it is in fact the form of kriging used most (Chilès and Delfiner, 1999). Goovaerts (1997) showed that the values in un-sampled locations are estimated by the ordinary kriging method according to moving average of the interest variables satisfying various distribution forms of data. It is a spatial estimation method where the error variance is minimized. This error variance is based on the configuration of the data and its variogram (Yamamoto, 2005). The correct variogram in kriging interpolation can guarantee the accuracy of the interpolation results.

The accuracy of the spatial interpolation analysis is verified by comparing the difference between the measured values and the predicted values, so as to select the best variogram model. In order to test the variogram model, the cross-validation method was used to determine whether the parameters of the variogram model are correct. The distribution of the residual is normal (Fig.7) and the mean of error between the actual and estimated Cu grade values is equal to 0 (Table 1). It indicates that this model is reasonable, and the variogram parameters are unbiased for estimating the Cu grade.

The obtained block models were used as input to the fractal models. The Pulang deposit was modeled by 20m × 20m × 5m voxels and they were decided by the grid drilling dimensions and geometrical properties of the deposit (David, 1970). The Pulang deposit is totally modeled with 150,973 voxels. The terms of “highly”, “moderately” and “weakly” have been used to classify the mineralized zones based on fractal modeling and accordance with the classification of in terms of ore grades in the deposit.

<Fig. 5 inserts here>

<Fig. 6 inserts here>

4.1. Concentration–volume (C–V) fractal modeling

The occupied volume values corresponding to Cu grades were computed to obtain the concentration–volume model according to the 3D model of Pulang deposit. Through the obtained C–V log–log plot, the threshold values of Cu grades were determined (Fig.8). It indicates the power-law relationship between Cu grades and volumes. Three thresholds and four populations were obtained from C–V log–log plot, consequently. The first Cu threshold is 0.25%. The range of Cu values of <0.25% represent barren host rocks. The second Cu threshold is 1.38%, and values of 0.25–1.38% Cu represent weakly grade mineralization zones. And the third Cu threshold is 1.88%. The range of Cu values of 1.38–1.88% denote moderately mineralized zones, and values of >1.88% Cu indicate highly mineralized zones (Table 2). According to the results, the low concentration zones exist in many parts of Pulang deposit and are disposed along the northwest–southeast trend of the deposit. Moderately and highly mineralized zones are located at several parts of the center and south of Pulang deposit (Fig. 9).

4.2. Power spectrum–volume (S–V) fractal modeling

According to the geological data, such as the collar coordinates, azimuth, dip, mineralogy and lithology recorded from 130 drill holes, a 3D model and block model of Cu distribution of Pulang deposit were constructed with ordinary kriging method using the Geovia Surpac software.

The power spectrum (S) were computed for the 3D elemental distribution utilizing 3D fast Fourier transformation by MATLAB (R2016a). The logarithmic values of power spectrums and relevant volume values were plotted against each other (Fig. 10). The straight lines fitted through the log–log plot indicate different relationships between power spectrums and occupied volumes. The results have indicated that there are two thresholds and three different power–law relationships. The thresholds of logS=7.81 and logS=8.70 were decided by the log–log S–V plot. The 3D filters were designed to separate different mineralization zones on the basis of these threshold values. Inverse fast Fourier transformation was used to convert the decomposed components back into the space domain by MATLAB (R2016a). According to the results, Cu concentrations of the hypogene zones range from 0.23% to 1.33% (Table 3), and values of >1.33% Cu refer to the supergene enrichment zones, whereas values of <0.23% Cu pertain to the leached zone and barren host rocks (Fig. 11).

<Fig. 9 inserts here>

<Fig. 10 inserts here>

< Table 2 inserts here>

5. Comparison of fractal models and geological model of the deposit

Alteration models have a key role in zone delineation and also in presenting geological models, as described by Lowell and Guilbert (1970). The potassic and phyllic alterations control major mineralization within supergene enrichment and hypogene zones according to these models. The models of various mineralization zones obtained by the fractal methods could be compared with geological data to validate these results.

Results of fractal models of Pulang deposit were in contrast with the 3D geological model of Pulang deposit constructed by utilizing Geovia Surpac software and drillholes data (Fig. 2). Furthermore, the results obtained from fractal models are also controlled by mineralogical investigations.

Carranza (2011) has illustrated an analysis for calculation of spatial correlations between two binary especially mathematical and geological models. An intersection operation between the mineralization zones obtained from fractal models and different alteration zones in the geological model was performed to derive the amount of voxels corresponding to each of the classes of overlap zones (Table 4). Using the obtained numbers of voxels, Type I error (T1E), Type II error (T2E), and overall accuracy (OA) of the fractal model were estimated with respect to different alteration zones due to geological data (Carranza, 2011). And the values of OA of fractal models of mineralized zones were compared with each other as follows.

The comparison between highly mineralized zones on the basis of the fractal models and potassic alteration zones resulted from the 3D geological model illustrates that the results of these two fractal models are similar. The overall accuracy values of C–V and S–V models are 0.50 and 0.52 as shown in Table 5, which illustrate that the S–V model gives more accurate results to recognize highly grade mineralization zones in Pulang deposit.

Comparison between phyllic alteration zones resulted from the 3D geological model and moderately grade mineralization zones obtained from fractal methods indicates that OA values of C–V and S–V fractal methods in regard to phyllic alteration zones of the geological model are 0.59 and 0.56 (Table 6). The OA values of moderately and weakly grade mineralization zones obtained from C–V model is higher than the results obtained from S–V model.

It could be considered that there are spatial correlations between different modeled Cu zones and geological features such as alterations and mineralogy. Several samples were collected from different drill holes in different grade mineralization zones of Pulang deposit to validate the results of fractal models. They were analyzed by microscopic identification and XRF (X-ray Fluorescence Spectrometer). PL-B82 sample was collected from the drill hole situated in the high grade mineralization zones. There are high chalcopyrite content and some molybdenite (Fig.14a). PL-B62 sample was collected from the drill hole situated in the moderate grade mineralization zones. There are low chalcopyrite content and some pyrrhotite content in polished section (Fig.14b). PL-B74 sample was collected from the drill hole located at the weakly mineralized zones with lower chalcopyrite content and some pyrrhotite (Fig.14c and Fig.14d). Results obtained from mineralogy, microscopic identification and drillcore scanning by XRF of these samples indicates that Cu concentrations are 1.80%,1.32% and 0.41% in PL-B82, PL-B62 and PL-B74 samples, respectively (Table 7).

6. Conclusions

In the many cases, drillcore logging in the field is dealing with the lack of proper diagnosis of geological phenomenon and it can undermine delineation of mineralized zones because it depends on the interpretation of individual loggers, which is subjective and no two loggers usually have the same interpretations. However, conventional geological modeling based on drillcore data is fundamentally important for ore body spatial structure understanding and mathematical applications. Grades of the ore elements are not observed in conventional methods of geological ore modeling while the variations in ore grades in a mineral deposit is an obvious and salient feature. Given the problems as mentioned above, using a series of newly established methods based on mathematical analyses such as fractal modeling seems to be inevitable.

This study utilized the concentration–volume (C–V) and power spectrum–volume (S–V) fractal models to delineate and recognize different grade Cu mineralization zones of Pulang copper deposit. Both the fractal models reveal high grade Cu mineralization zones is located at the central and southern parts of Pulang deposit. The Cu threshold of high grade mineralization zones is 1.88% according to C–V method. And Cu threshold of supergene enrichment zones is 1.33% on the basis of S–V method. Models of moderate grade mineralization zones contain 1.38–1.88% Cu according to the C–V method. And the hypogene zones contain 0.23–1.33% Cu according to the S–V model. The C–V method shows barren host rocks include <0.25% and weak grade mineralization include 0.25–1.38% Cu. And the S–V model reveals that barren host rock and leached zone contain <0.23% Cu.

Carranza (2011) has illustrated an analysis for calculation of spatial correlations between two binary especially mathematical and geological models. An intersection operation between the mineralization zones obtained from fractal models and different alteration zones in the geological model was performed to derive the amount of voxels corresponding to each of the classes of overlap zones. Using the obtained numbers of voxels, Type I error (T1E), Type II error (T2E), and overall accuracy (OA) of the fractal models were estimated with respect to different alteration zones due to geological data. And the values of OA of fractal models of mineralized zones were compared with each other.

The comparison between highly mineralized zones based on the fractal models and potassic zones resulted from 3D geological model illustrates that the S–V fractal model is better than the C–V model because the fact that the number of overlapped voxels (A) in the S–V model is higher than those in the C–V model. The overall accuracy values of C–V and S–V fractal models with respect to the potassic alteration zones of the geological model are 0.50 and 0.52, which illustrate that the S–V model gives better results to recognize high grade mineralization zones in Pulang deposit. On the other hand, correlation (from OA results) between highly mineralized zones obtained from S–V modeling and the potassic alteration zones is higher than the C–V model because of a strong proportional relationship between extension and positions of voxels in the S–V model and potassic alteration zones in the 3D geological model.

Comparison between phyllic alteration zones resulted from the 3D geological model and moderate grade mineralization zones obtained from fractal methods indicates that OA values of C–V and S–V fractal methods in regard to phyllic alteration zones of the geological model are 0.59 and 0.56, respectively. The OA values of moderate and weak grade mineralization zones obtained from C–V model is higher than the results obtained by S–V model. On the other hand, moderately mineralized zones defined by C–V modeling have overlap with the phyllic alteration zones in the 3D geological model. However, the outcomes of the C–V model are more accurate than those of the S–V model with respect to the phyllic alteration zones in the 3D geological model.

According to the correlation between results driven by fractal modeling and geological logging from drill holes in the Pulang porphyry copper deposit, high grade mineralization zones generated by fractal models, especially the S–V model, have a better correlation with potassic alteration zones resulted from the 3D geological model than the C–V model. And moderately mineralized zones correlate with phyllic alteration zones in the central and southern parts of the Pulang deposit. There is a better relationship between moderately and weakly mineralized zones derived by the C–V model and the phyllic alteration zones according to the 3D geological model than the S–V model.

Acknowledgements

This research was supported by the National Key R&D Program of China (2016YFC0600508). The authors thank Tao Dong, Haijun Yu, Qiwu Shen, Zhipeng Li, Baosheng Shi and Jinhong Yang for supporting in field investigation and providing parts of raw data.

References

Agterberg, F.P., Cheng, Q., and Wright, D.F.: Fractal modeling of mineral deposits,in:Proceedings of the 24th APCOM Symposium, Montreal, Canada,43–53, 1993.

Agterberg, F.P.: Multifractal modeling of the sizes and grades of giant and supergiant deposits, International Geology Review, 37,1–8, https://doi.org/10.1080/ 00206819509465388 , 1995.

Afzal, P., Fadakar Alghalandis, Y., Khakzad, A., Moarefvand, P., and Rashidnejad Omran, N.: Delineation of mineralization zones in porphyry Cu deposits by fractal concentration–volume modeling, J. Geochem. Explor., 108, 220–232, https://doi.org/ 10.1016/j.gexplo.2011.03.005, 2011.

Afzal, P., Fadakar Alghalandis, A., Moarefvand, P., Rashidnejad Omran, N., and Asadi Haroni, H.: Application of power–spectrum–volume fractal method for detecting hypogene, supergene enrichment, leached and barren zones in Kahang Cu porphyry deposit, Central Iran, J. Geochem. Explor., 112, 131–138, https://doi.org/10.1016/ j.gexplo.2011.08.002, 2012.

Beane, R.E.: Hydrothermal alteration in silicate rocks, in: Advances in Geology of the Porphyry Copper Deposits, Southwestern NorthAmerica, Titley, S.R. (Ed.),The University of Arizona Press, Tucson, 117–137, 1982.

Bolviken, B., Stokke, P.R., Feder, J., and Jossang, T.: The fractal nature of geochemical landscapes, J. Geochem. Explor., 43,91–109,https://doi.org/10.1016/ 0375-6742(92)90001-O, 1992.

Boyce, A.J., Fulgnati, P., Sbrana, A., and Fallick, A.E.: Fluids in early stage hydrothermal alteration of high-sulfidation epithermal systems: a view from the volcano active hydrothermal system (Aeolian Island, Italy), Journal of Volcanology and Geothermal Research, 166, 76–90,https://doi.org/10.1016/j.jvolgeores. 2007.07.005, 2007.

Berger, B. R., Ayuso, R. A., Wynn, J. C., and Seal, R. R.: Preliminary Model of Porphyry Copper Deposits, USGS, Open-File Report, 1321 pp., 2008.

Cox, D. and Singer, D.: Mineral deposits models, US GeologicalSurvey Bulletin, 1693 pp., 1986.

Craig, G.R. and Vaughan, D.: Ore Microscopy and Ore Petrography, John Wiley andSons, 1994.

Chilès, J.P. and Delfiner, P.: Geostatistics: Modeling Spatial Uncertainty, Wiley, NewYork, 695 pp., 1999.

Carranza, E.J.M.: Geochemical Anomaly and Mineral Prospectivity Mapping inGIS. Handbook of Exploration and Environmental Geochemistry,11, Amsterdam, Elsevier, 351 pp., 2008.

Carranza, E. J. M.: Controls on mineral deposit occurrence inferredfrom analysis of their spatial pattern and spatial association withgeological features, Ore Geol. Rev., 35, 383–400, https://doi.org/10.1016/j.oregeorev.2009.01.001, 2009.

Carranza, E.J.M., Owusu, E.A., and Hale, M.: Mapping of prospectivity and estimation of number of undiscovered prospects for lode gold, southwestern Ashanti Belt, Ghana, Mineralium Deposita, 44, 915–938, https://doi.org/10.1007/s00126-009-0250-6, 2009.

Carranza, E.J.M.: From predictive mapping of mineral prospectivity to quantitative estimation of number of undiscovered prospects. Resource Geology 61, 30–51, 2010.

Carranza, E.J.M.: Analysis and mapping of geochemical anomalies using logratio-transformed stream sediment data with censored values, J. Geochem. Explor., 110, 167–185, https://doi.org/10.1016/j.gexplo.2011.05.007, 2011.

Cheng, Q., Agterberg, F.P., and Ballantyne, S.B.: The separation of geochemical anomaliesfrom backgroundby fractal methods, J. Geochem. Explor., 51, 109–130, https://doi.org/10.1016/0375-6742(94)90013-2, 1994.

Cheng, Q.: Spatial and scaling modelling for geochemical anomaly separation, J. Geochem. Explor., 65, 175–194, https://doi.org/10.1016/S0375-6742(99)00028-X, 1999.

Cheng, Q.: Multifractal modelling and spectrum analysis: methods and applications to gamma ray spectrometer data from southwestern Nova Scotia, Canada, Science in China, Series D: Earth Sciences 49 (3), 283–294, 2006.

Cheng, Q.: Mapping singularities with stream sediment geochemical data forprediction of undiscovered mineral deposits in Gejiu, Yunnan Province, China, Ore Geol. Rev., 32, 314–324,https://doi.org/10.1016/j.oregeorev.2006.10.002, 2007.

David, M.: Geostatistical Ore Reserve Estimation, Amsterdam, Elsevier, 283 pp., 1970.

Deng, J., Wang,C.M., and Li,G.J.: Style and processofthesuperimposedmineralization inthe Sanjiang Tethys, Acta Petrologica Sinica, 28 (5), 1349–1361 (in Chinese with Englishabstract), 2012.

Deng, J., Wang, Q.F., Li, G.J., and Santosh, M.: Cenozoic tectono-magmatic andmetallogenic processes in the Sanjiang region, southwestern China, Earth Sci. Rev., 138, 268–299,https://doi.org/10.1016/j.earscirev.2014.05.015, 2014a.

Deng, J., Wang, Q.F., Li, G.J., Li, C.S., and Wang, C.M.: Tethys tectonic evolution and itsbearing on the distribution of important mineral deposits in the Sanjiang region,SW China, Gondwana Research, 26 (2), 419–437,https://doi.org/10.1016/ j.gr.2013.08.002, 2014b.

Deng, J., Wang, Q.F., Li, G.J., Hou, Z.Q., Jiang, C.Z., and Danyushevsky, L.: Geology andgenesis of the giant Beiya porphyry–skarn gold deposit, northwestern YangtzeBlock, China, Ore Geol. Rev., 70, 457–485,https://doi.org/10.1016/ j.oregeorev. 2015.02.015, 2015.

Faure, K., Matsuhisa, Y., Metsugi, H., Mizota, C., and Hayashi, S.: The Hishikari Au–Agepithermal deposit, Japan: oxygen and hydrogen isotope evidence in determiningthe source of paleohydrothermal fluids, Economic Geology, 97, 481–498, https://doi.org/10.2113/gsecongeo.97.3.481, 2002.

Goovaerts, P.: Geostatistics for Natural Resources Evaluation, Oxford UniversityPress, New York, 496 pp. , 1997.

Goncalves, M. A., Mateus, A., and Oliveira, V.: Geochemicalanomaly separation by multifractal modeling, J. Geochem. Explor., 72, 91–114,https://doi.org/10.1016/ S0375-6742(01)00156-X, 2001.

Lowell, J.D.: Geology of the Kalamazoo orebody, San Manuel district, Arizona, Economic Geology, 63, 645–654, https://doi.org/10.2113/gsecongeo.63.6.645, 1968.

Lowell, J.D. and Guilbert, J.M.: Lateral and vertical alteration-mineralization zoning inporphyry ore deposits, Economic Geology, 65, 373–408, https://doi.org/10.2113/gsecongeo.65.4.373, 1970.

Li, C., Ma, T., and Shi, J.: Application of a fractal method relating concentrations anddistances for separation of geochemical anomalies from background, J. Geochem. Explor.,77, 167–175,https://doi.org/10.1016/S0375-6742(02)00276-5, 2003.

Li, W.C., Zeng, P.S., Hou, Z.Q., and White, N.C.: The Pulang porphyry copper deposit andassociated felsic intrusions in Yunnan Province, Southwest China, Economic Geology, 106 (1),79–92,https://doi.org/10.2113/econgeo.106.1.79 , 2011.

Leng, C.B., Zhang, X.C., Hu, R.Z., Wang, S.X., Zhong, H., Wang, W.Q., and Bi, X.W.: ZirconU–Pb and molybdenite Re–Os geochronology and Sr–Nd–Pb–Hf isotopic constraintson the genesis of the Xuejiping porphyry copper deposit in Zhongdian, NorthwestYunnan, China, Journal of Asian Earth Sciences ,60, 31–48, 2012.

Liu, X.L., Li, W.C., Yin, G.H., and Zhang, N.: The geochronology, mineralogy and geochemistry study of the Pulang porphyry copper deposits in Geza arc of Yunnan Province, Acta Petrologica Sinica, 29(9), 3049–3064 (in Chinese with English abstract), 2013.

Mandelbrot, B. B.: The Fractal Geometry of Nature, W. H. Freeman, San Fransisco, 468 pp., 1983.

Melfos,V., Vavelidis,M., Christodes,G., and Seidel,E.: Origin and evolution of the Tertiary Maronia porphyry copper–molybdenum deposit, Thrace, Greece, Mineralium Deposita, 37, 648–668,https://doi.org/10.1007/s00126-002-0277-4, 2002.

Mao, J.W., Zhou, Z.H., Feng, C.Y., Wang, Y.T., Zhang, C.Q., Peng, H.J., and Yu, M.: A preliminary study of the Triassic large-scale mineralization in China and its geodynamicsetting, Geology in China, 39(6), 1437–1471 (in Chinese with English abstract), 2012.

Mao, J.W., Pirajno, F., Lehmann, B., Luo, M.C., and Berzina, A.: Distribution of porphyrydeposits in the Eurasian continent and their corresponding tectonic settings, Journal of Asian Earth Sciences, 79(PartB), 576–584, https://doi.org/10.1016/j.jseaes.2013.09.002, 2014.

Pang, Z.S., Du, Y.S., Wang, G.W., Guo, X., Cao, Y., and Li, Q.: Single-grain zircon U–Pb isotopic ages, geochemistry and its implication of Pulang complex in Yunnan Province,China, Acta Petrologica Sinica, 25(1), 159–165(in Chinese with English abstract), 2009.

Pyrcz, M.J. and Deutsch, C.V.: Geostatistical ReservoirModeling, OxfordUniversity Press, 2014.

Schwartz, G.M.: Hydrothermal alteration in the "porphyry copper" deposits, Economic Geology, 42, 319–352, https://doi.org/10.2113/gsecongeo.42.4.319, 1947.

Sillitoe, R.H. and Gappe, I.M.: Philippine porphyry copper deposits: geologic settingand characteristics, Common Coordination Joint Resource (CCOP),14, 1–89, 1984.

Sillitoe, R.H.: Characteristics and controls of the largest porphyry copper–gold andepithermal gold deposits in the circum-pacific region, Australian Journal of Earth Sciences, 44, 373–388, https://doi.org/10.1080/08120099708728318, 1997.

Sim, B.L., Agterberg, F.P., and Beaudry, C.: Determining the cutoff between background and relative base metal contamination levels using multifractal methods, Comput. Geosci., 25, 1023–1041,1999.

Sadeghi, B., Moarefvand, P., Afzal, P., Yasrebi, A.B., and Saein, L.D.: Application of fractalmodels to outline mineralized zones in the Zaghia iron ore deposit, Central Iran, J. Geochem. Explor., 122, 9–19,https://doi.org/10.1016/j.gexplo.2012.04.011, 2012.

Soltani, F., Afzal, P., and Asghari, O.: Delineation of alteration zones based on SequentialGaussian Simulation and concentration–volume fractal modeling in the hypogenezone of Sungun copper deposit, NW Iran, J. Geochem. Explor., 140, 64–76, https://doi.org/10.1016/j.gexplo.2014.02.007, 2014.

Sun, T. and Liu, L.: Delineating the complexity of Cu-Mo mineralization in a porphyryintrusion by computational and fractal modeling: A case study of the Chehugoudeposit in the Chifeng district, Inner Mongolia, China, J. Geochem. Explor., 144,128–143,https://doi.org/10.1016/j.gexplo.2014.02.015, 2014.

Turcotte, D.L.: A fractal approach to the relationship between ore grade andtonnage, Economic Geology, 18, 1525–1532, 1986.

Turcotte, D.L.: Fractals in geology and geophysics, Pure Appl.Geophys., 131, 171–196, 1989.

White, N.C. and Hedenquist, J.W.: Epithermal gold deposits: styles, characteristicsand exploration, SEG Newsletter, 23, 1–14, 1995.

Wilson, A.J., Cooke, David, R., Harper, B.J., and Deyell, C.L.: Sulfur isotopic zonation inthe Cadia district, southeastern Australia: exploration significance and implications for the genesis of alkalic porphyry gold–copper deposits, Mineralium Deposita, 42, 465–487,https://doi.org/10.1007/s00126-006-0071-9, 2007.

Wang, Q.F., Deng, J., Liu, H., Wang, Y., Sun, X., and Wan, L.: Fractal models for estimating local reserves with different mineralization qualities and spatial variations, J. Geochem. Explor., 108, 196–208, https://doi.org/10.1016/j.gexplo.2011.02.008, 2011.

Wang, Q.F., Deng, J., Li, C.S., Li, G.J., Yu, L., and Qiao, L.: The boundary between the Simaoand Yangtze blocks and their locations in Gondwana and Rodinia: constraints from detrital and inherited zircons, Gondwana Research, 26(2), 438–448,https://doi.org/10.1016/j.gr.2013.10.002, 2014.

Wang, G. W., Emmanuel John M. Carranza,Zuo, R., Hao, Y. L., Du, Y. S., Pang, Z. S., and Sun Y.: Mapping of district-scale potential targets using fractal models, J. Geochem. Explor., 122, 34–46,https://doi.org/10.1016/j.gexplo.2012.06.013, 2012.

Yamamoto, J.K.: Comparing Ordinary Kriging Interpolation Variance and Indicator Kriging Conditional Variance for Assessing Uncertainties at Unsampled Locations, in: Application ofComputers and Operations Research in the Mineral Industry,edited by: Dessureault, S., Ganguli, R., Kecojevic, V., and Girard-Dwyer, J., Balkema, 2005.

Yunnan Diqing Nonferrous Metal Co. Ltd.: Exploration Report of Pulang Copper Deposit, Diqing, Yunnan, China, Yunnan Diqing Nonferrous Metal Co. Ltd., DiqingTibetan Autonomous Prefecture (in Chinese), 2009.

Zeng, P.S., Hou, Z.Q., Li, L.H., Qu, W.J., Wang, H.P., Li, W.C., Meng, Y.F., and Yang, Z.S.: Age of the Pulang porphyry copper deposit in NW Yunnan and its geological significance, Geological Bulletin of China, 23(11), 1127–1131 (in Chinese with English abstract), 2004.

Zuo, R., Cheng, Q., and Xia, Q.: Application of fractal models to characterization of vertical distribution of geochemical element concentration, J. Geochem. Explor., 102, 37–43,https://doi.org/10.1016/j.gexplo.2008.11.020, 2009.

Zuo, R. and Wang, J.: Fractal/multifractal modeling of geochemical data: A review, J. Geochem. Explor., 164, 33-41, https://doi.org/10.1016/j.gexplo.2015.04.010, 2016.

Fig.1. Geological map of the Pulang porphyry copper deposit, SW China.Modified after Yunnan Diqing Nonferrous Metal Co. Ltd., 2009.

Fig.2. Geological 3D models including lithology, alterationand 3Ddrillholeplot with the legend of each in thePulang porphyry copper deposit. (Scale is in m^3.)

Fig.3. Photographs of alteration and mineralization in the Pulang porphyry copper deposit, SW China. (a) Quartz monzonite porphyry with potassium-silicate alteration; (b) Quartz diorite porphyrite with quartz-sericite alteration; (c) Quartz diorite porphyrite with propylitic alteration; (d) Hornfels. Qtz=quartz; Pl=plagioclase; Kfs=K-feldspar; Bt=biotite; Ser=sericite; Chl=chlorite; Ep=epidote; Py=pyrite; Ccp=chalcopyrite; Mo=molybdenite; Po= pyrrhotite.

Fig.4. Cross section along exploration line 0 in the Pulang porphyry copper deposit, SW China. Modified after Wang et al., 2012.

Fig.5. Histograms of the Cu raw (a) and logarithmic transformation (b) data in the Pulang deposit.

Fig.6. The experimental semi–variogram (omni-directional) of Cu data in Pulang deposit.

Fig.7. The cross-validation results: (a) residual VS Cu grade;(b) the residual distribution histogram.

Fig.8. C–V log–log plot for Cu concentrations in the Pulang deposit.

Fig.9. Zones in the Pulang deposit based on thresholds defined from the C–V fractal model of Cu data: (a) highly mineralized zones; (b) moderately mineralized zones; (c) weakly mineralized zones; (d) barren host rock.(Scale is in m^3.)

Fig.10. S–V log–log plot for Cu concentrations in the Pulang deposit.

Fig.11. Zones in the Pulang deposit based on thresholds defined from the S–V fractal model of Cu data: (a) the supergene enrichment zones; (b) the hypogene zones; (c) the leached zone and barren host rock (Scale is in m^3.)

Fig.12. Highly mineralized zones in the Pulang deposit: (a) potassium-silicate zone resulted from the 3D geological model from drillcore geological data; (b) C–V modeling of Cu data; and (c) S–V modeling of Cu data(Scale is in m^3.)

Fig.13. Moderately mineralized zones in the Pulang deposit:(a) quartz–sericite zones resulted from the 3D geological model from drillcore geological data; (b) C–V modeling of Cu data; and (c)S–V modeling of Cu data (Scale is in m^3.)

Fig.14. Chalcopyrite content in several samples based on mineralographical study: (a) PL-B82 sample was collected from the drill hole situated in the high grade mineralization zones.; (b) PL-B62 sample was collected from the drill hole situated in the moderately grade mineralization zones.; (c) and (d) PL-B74 sample was collected from the drill hole located at the weakly mineralized zones.

Table 1 The results of statistical characteristics of the residual.

Table 2 Thresholds concentrations obtained by using C–V model based on Cu% in Pulang deposit.

Table 3 Ranges of power spectrum (S) for different mineralization zones in Pulang deposit.

Table 4 Matrix for comparing performance of fractal modeling results with geological model. A, B, C, and D represent numbers of voxels in overlaps between classes in the binary geological model and the binary results of fractal models (Carranza, 2011).

Table 5 Overall accuracy (OA), Type I and Type II errors (T1E and T2E, respectively) with respect to potassic alteration zone resulted from geological model and threshold values of Cu obtained through C–V and S–V fractal modeling.

Table 6 Overall accuracy (OA), Type I and Type II errors (T1E and T2E, respectively) with respect to phyllic alteration zone resulted from geological model and threshold values of Cu obtained through C–V and S–V fractal modeling.

Table 7 Results of XRF analysis of samples collected from different mineralized zones in the Pulang porphyry copper deposit.

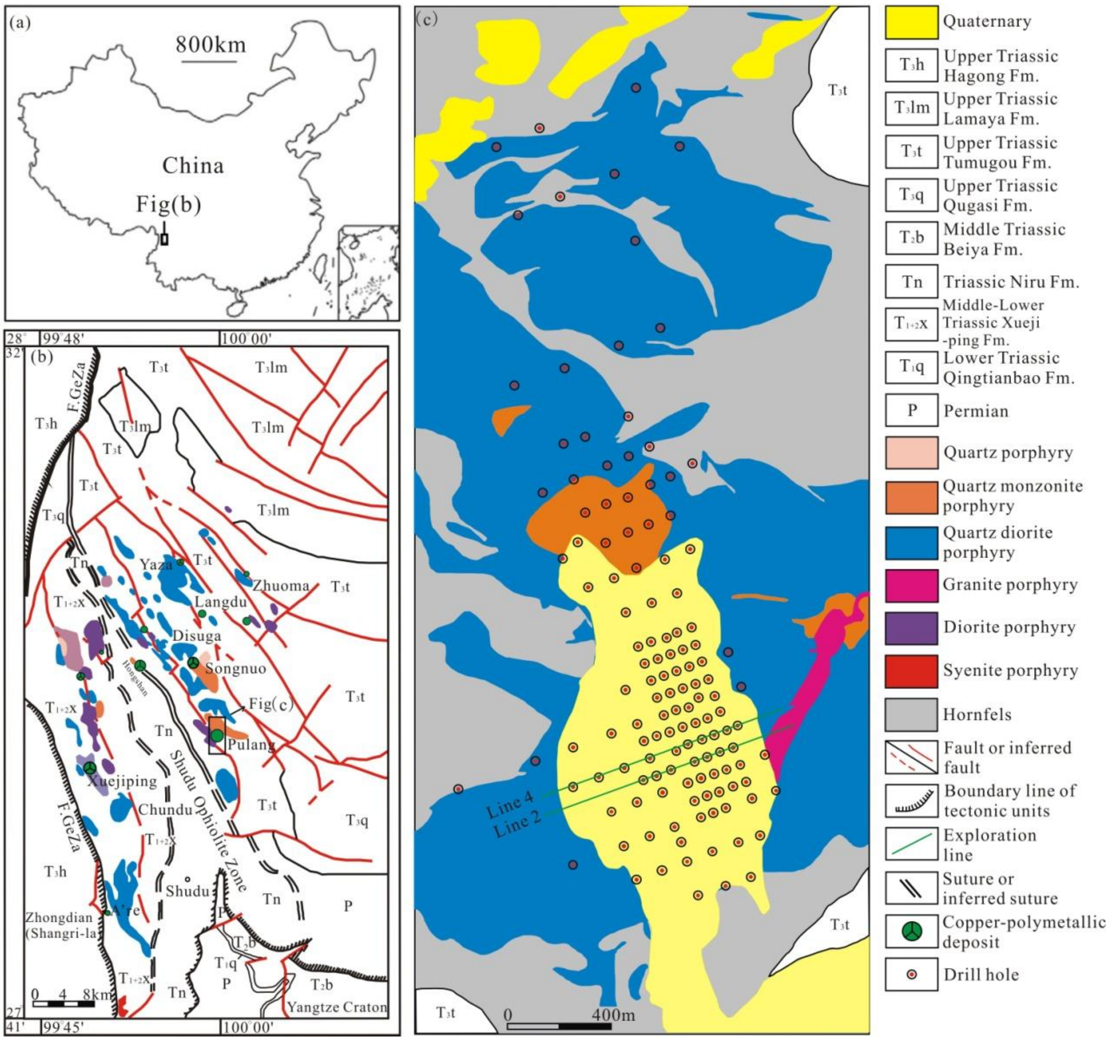
(a)
800km
China
Fig(b)
(b)
F.GeZa
Shudu Ophiolite Zone
Yaza
Zhuoma
Langdu
Disuga
Songnuo
Fig(c)
Pulang
Xuejiping
Chundu
Shudu
Zhongdian (Shangri-la)
Yangtze Craton
0 4 8km
99°45'
99°48'
100°00'
(c)
Line 4
Line 2
0 400m
Quaternary
Upper Triassic Hagong Fm.
Upper Triassic Lamaya Fm.
Upper Triassic Tumugou Fm.
Upper Triassic Qugasi Fm.
Middle Triassic Beiya Fm.
Triassic Niru Fm.
Middle-Lower Triassic Xuejiping Fm.
Lower Triassic Qingtianbao Fm.
Permian
Quartz porphyry
Quartz monzonite porphyry
Quartz diorite porphyry
Granite porphyry
Diorite porphyry
Syenite porphyry
Hornfels
Fault or inferred fault
Boundary line of tectonic units
Exploration line
Suture or inferred suture
Copper-polymetallic deposit
Drill hole

Fig. 1.

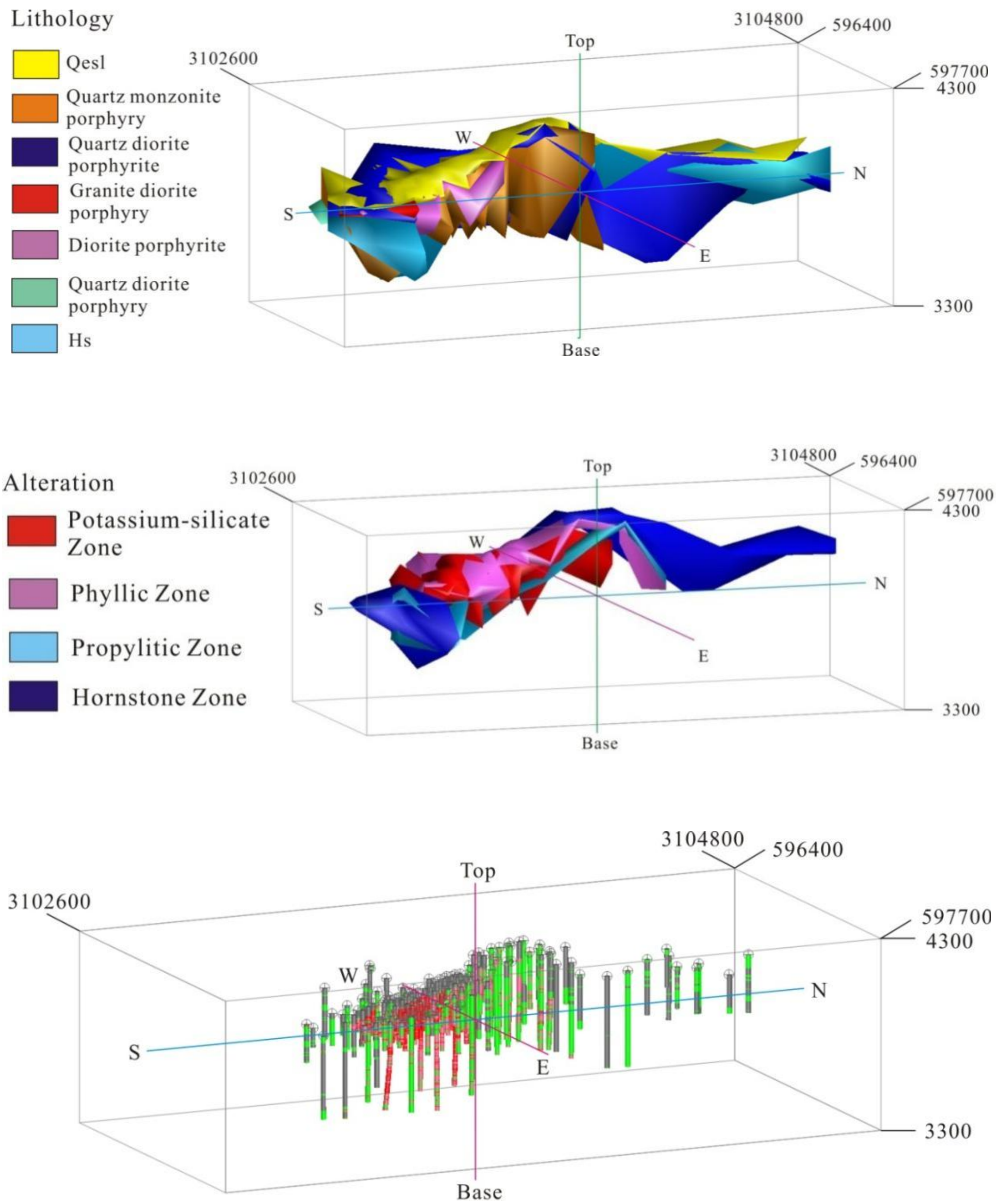
Lithology
Qesl
Quartz monzonite porphyry
Quartz diorite porphyrite
Granite diorite porphyry
Diorite porphyrite
Quartz diorite porphyry
Hs
3102600
3104800
596400
597700
4300
3300
Top
Base
W
E
S
N
Alteration
Potassium-silicate Zone
Phyllic Zone
Propylitic Zone
Hornstone Zone

Fig. 2.

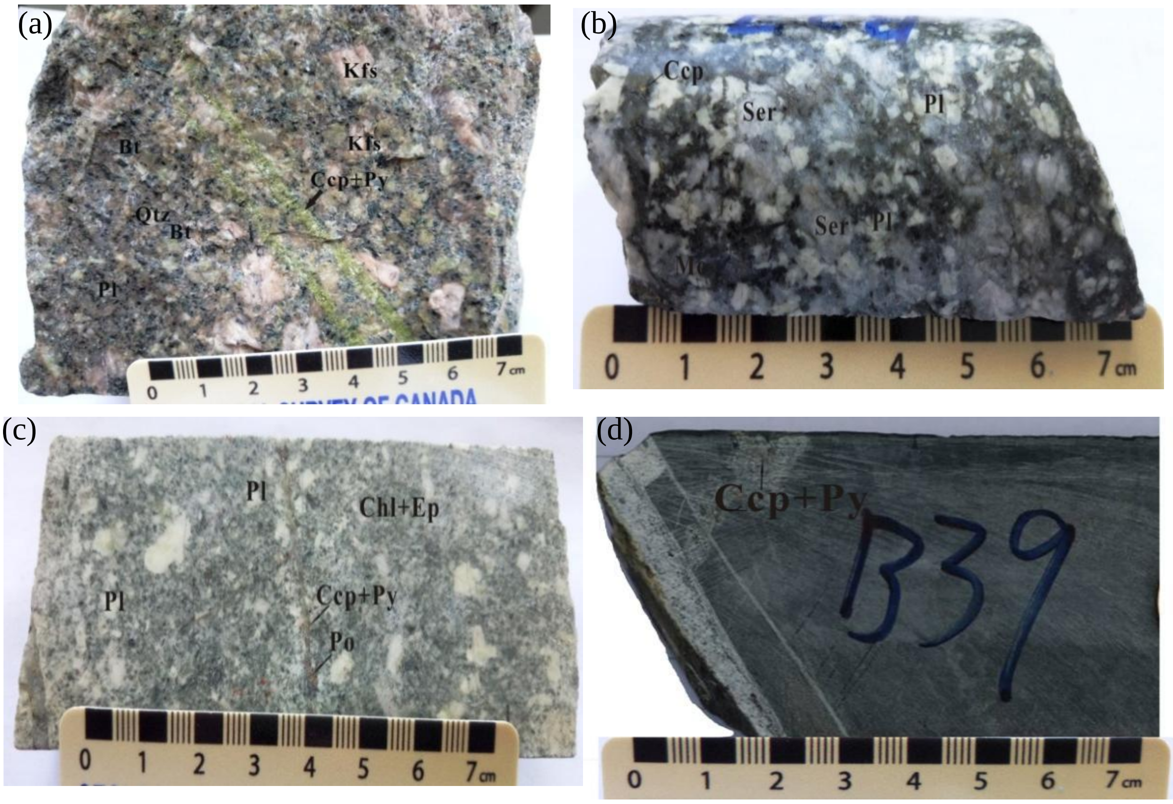
(a)
Kfs
Kfs
Bt
Ccp+Py
Qtz
Bt
Pl
(b)
Ccp
Ser
Pl
Ser
Pl
(c)
Pl
Chl+Ep
Pl
Ccp+Py
Po
(d)
Ccp+Py
B39

Fig. 3.

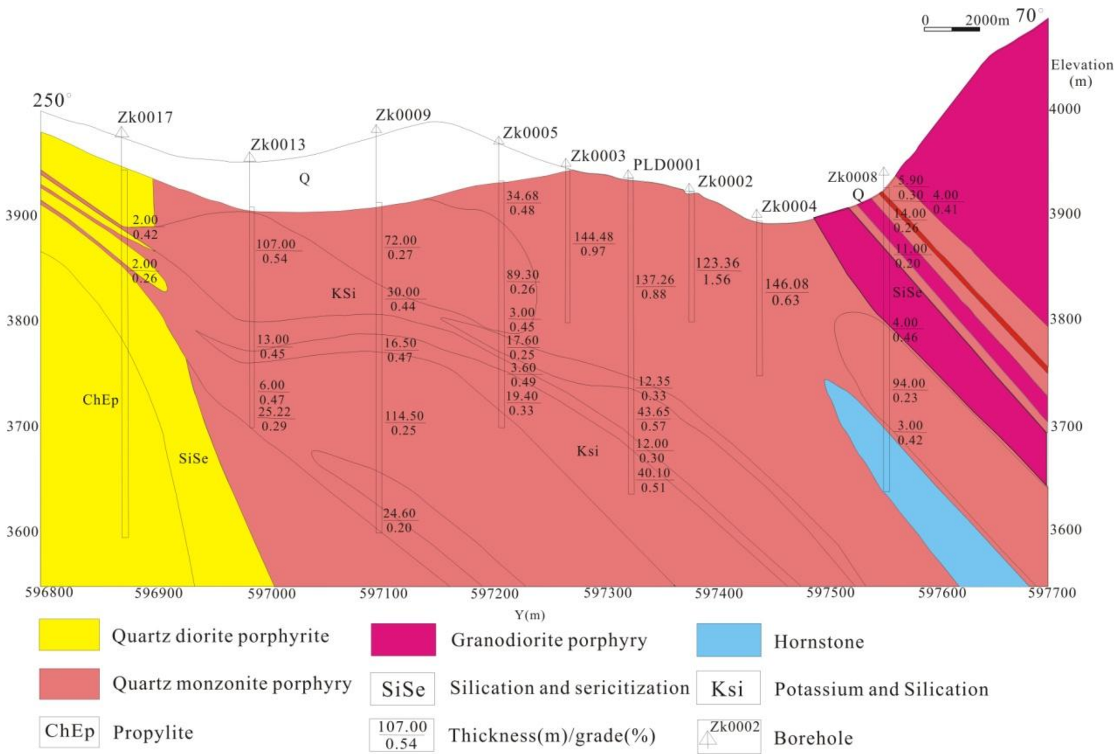
0 2000m
250°
70°
Elevation (m)
Zk0017
Zk0013
Zk0009
Zk0005
Zk0003
PLD0001
Zk0002
Zk0004
Zk0008
Q
KSi
Ksi
ChEp
SiSe
Y(m)
Quartz diorite porphyrite
Quartz monzonite porphyry
ChEp Propylite
Granodiorite porphyry
SiSe Silication and sericitization
107.00 / 0.54 Thickness(m)/grade(%)
Hornstone
Ksi Potassium and Silication
Zk0002 Borehole

Fig. 4.

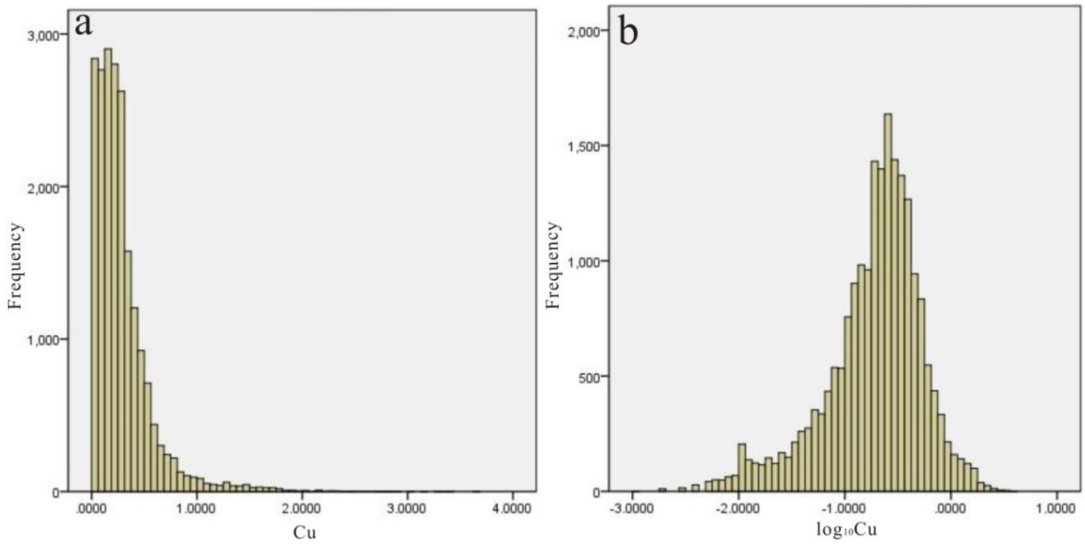

Fig. 5.

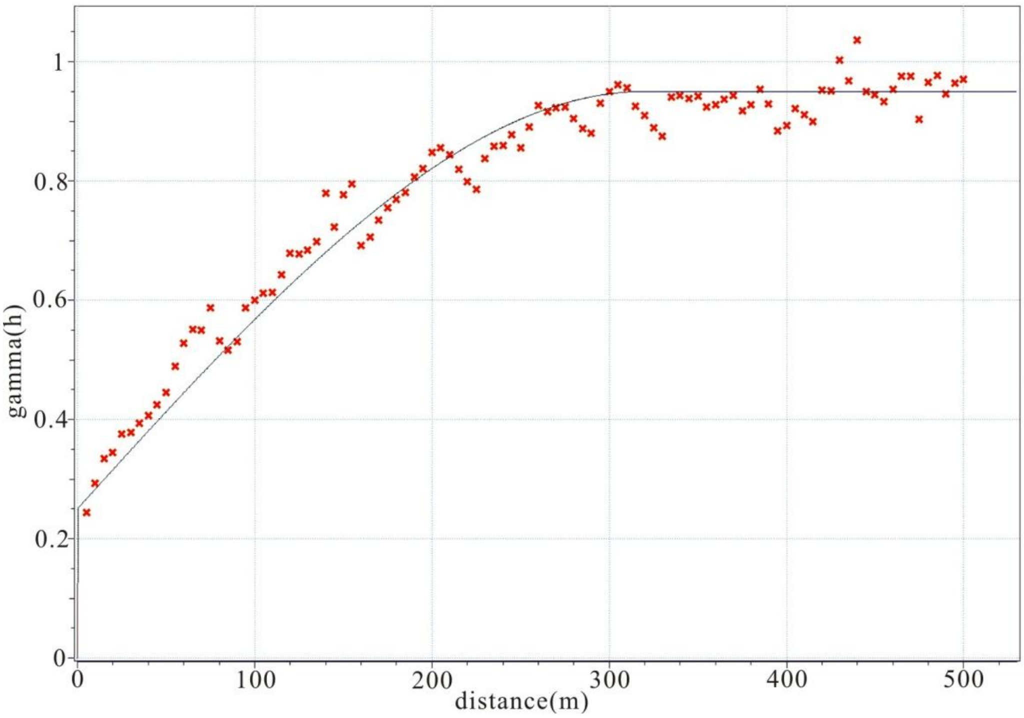

Fig. 6.

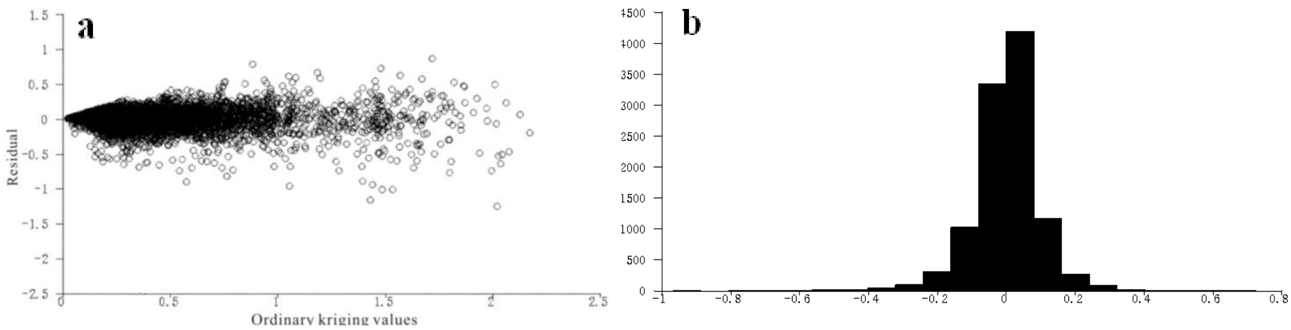

Fig. 7.

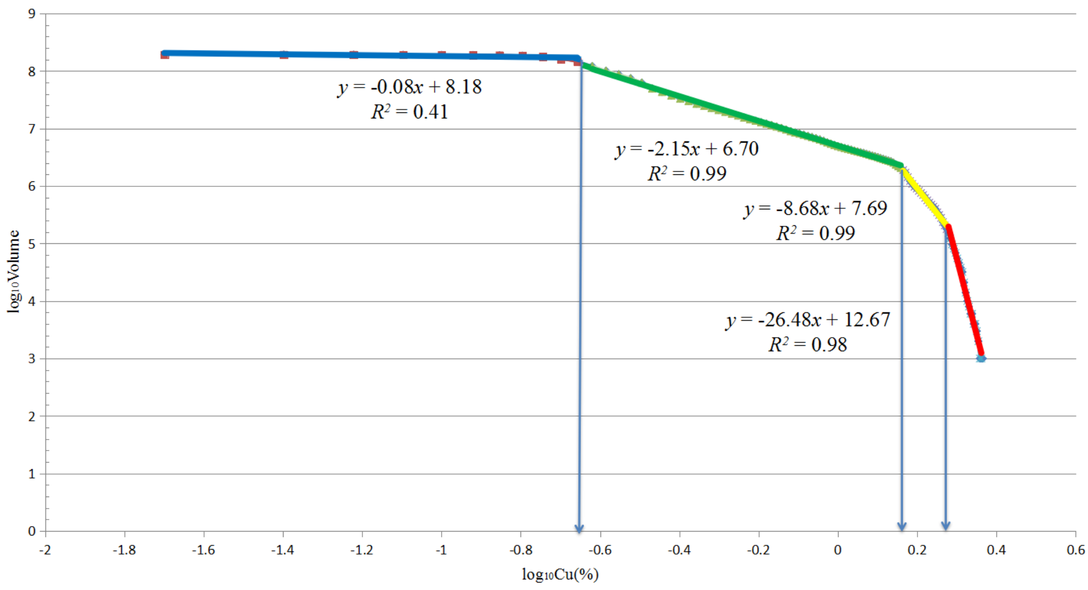

y = -0.08x + 8.18
R² = 0.41
y = -2.15x + 6.70
R² = 0.99
y = -8.68x + 7.69
R² = 0.99
y = -26.48x + 12.67
R² = 0.98
log₁₀Volume
log₁₀Cu(%)
0
1
2
3
4
5
6
7
8
9
-2
-1.8
-1.6
-1.4
-1.2
-1
-0.8
-0.6
-0.4
-0.2
0
0.2
0.4
0.6

Fig. 8.

(a)

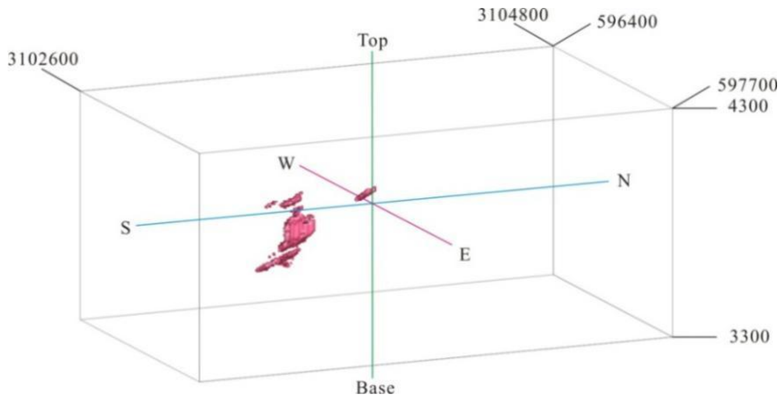
3104800
596400
Top
3102600
597700
4300
W
N
S
E
3300
Base

(b)

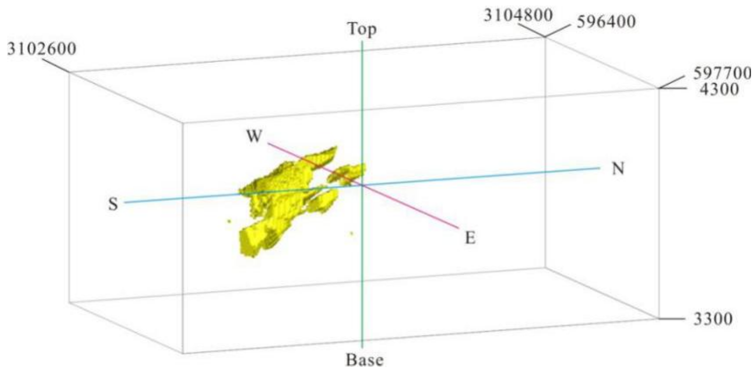
3104800
596400
Top
3102600
597700
4300
W
N
S
E
3300
Base

(c)

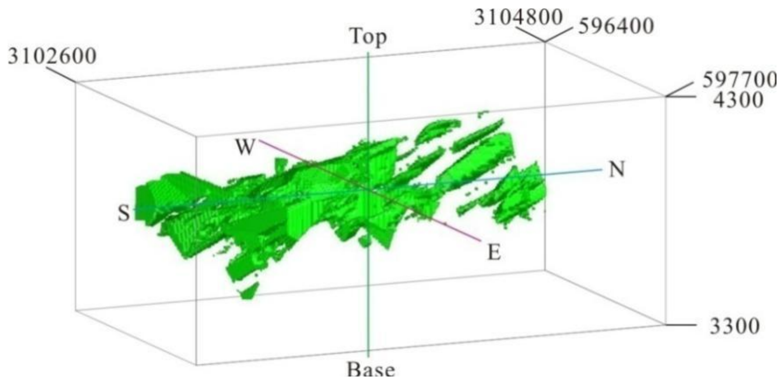
3104800
596400
Top
3102600
597700
4300
W
N
S
E
3300
Base

(d)

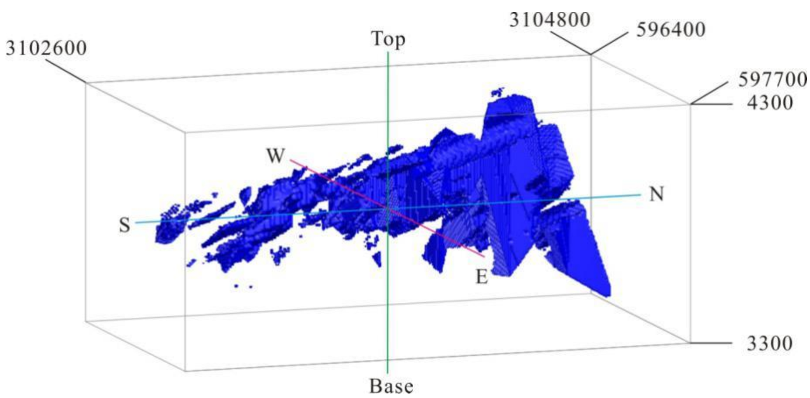
3104800
596400
Top
3102600
597700
4300
W
N
S
E
3300
Base

Fig. 9.

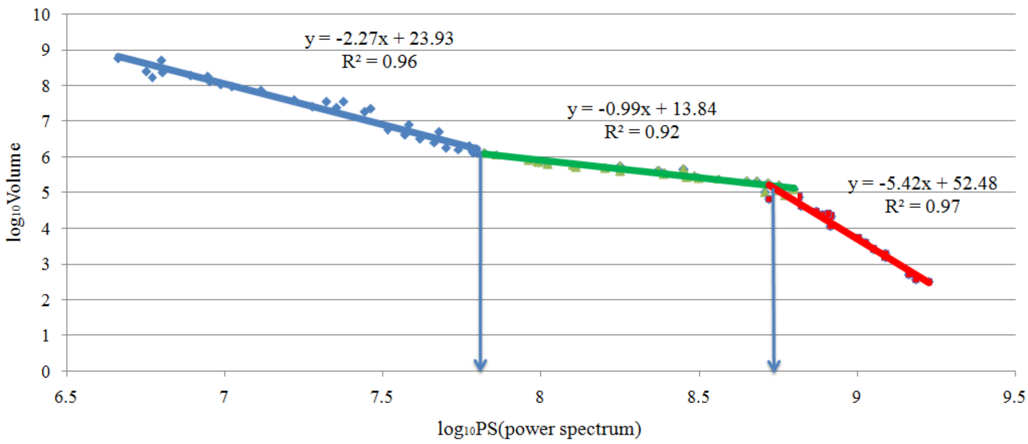

Fig. 10.

(a)

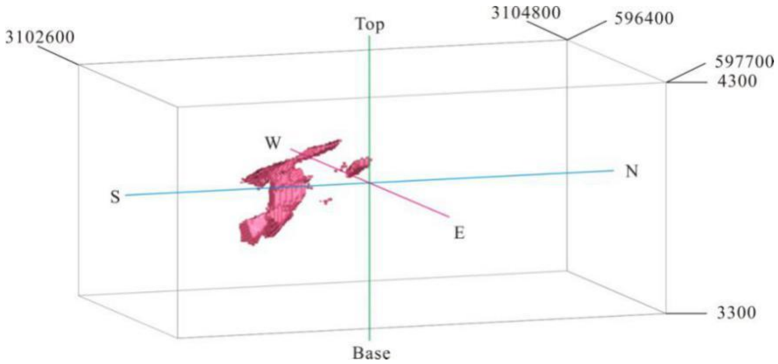

(b)

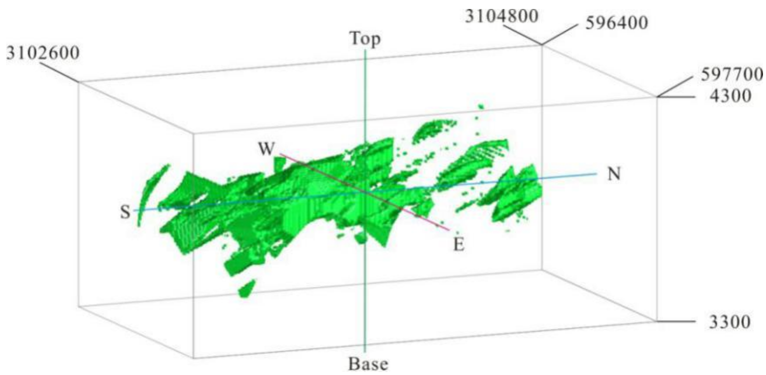

(c)

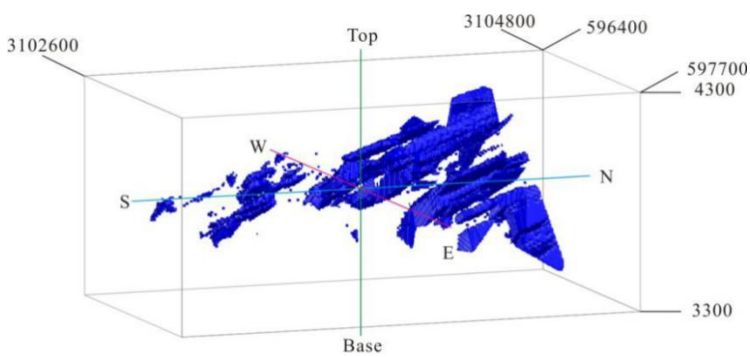

Fig. 11.

(a)

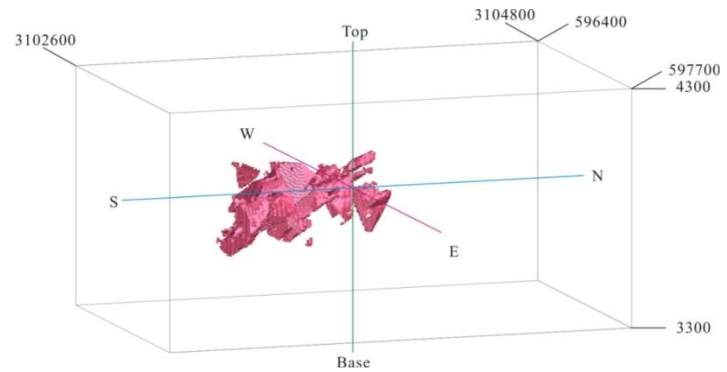

3102600
Top
3104800
596400
597700
4300
W
S
N
E
3300
Base

(b)

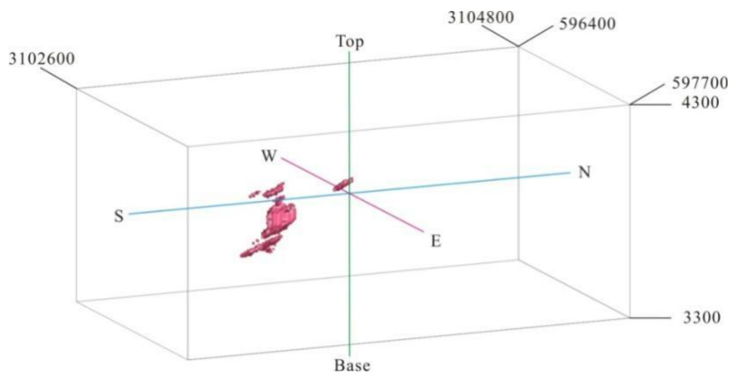

3102600
Top
3104800
596400
597700
4300
W
S
N
E
3300
Base

(c)

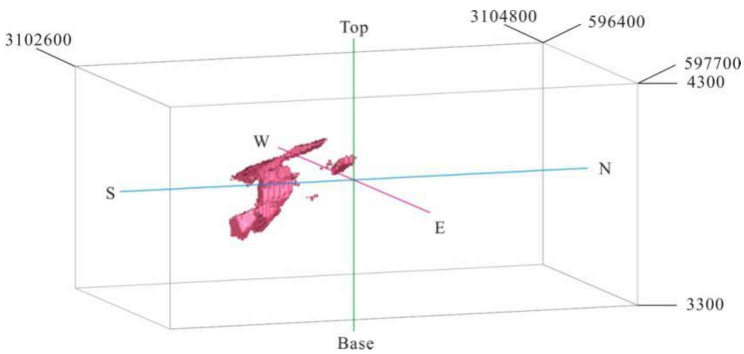

3102600
Top
3104800
596400
597700
4300
W
S
N
E
3300
Base

Fig. 12.

(a)

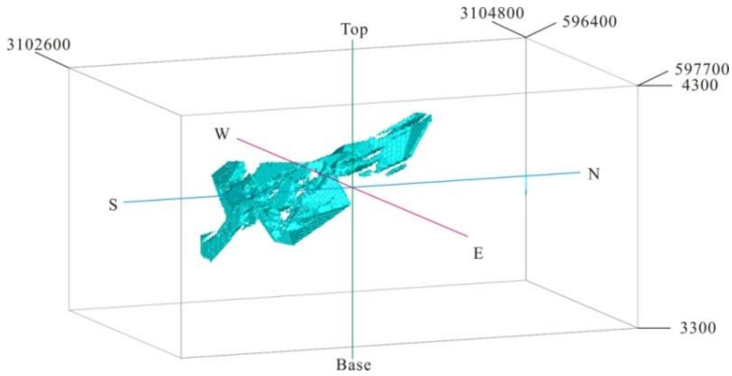
3102600
Top
3104800
596400
597700
4300
W
N
S
E
3300
Base

(b)

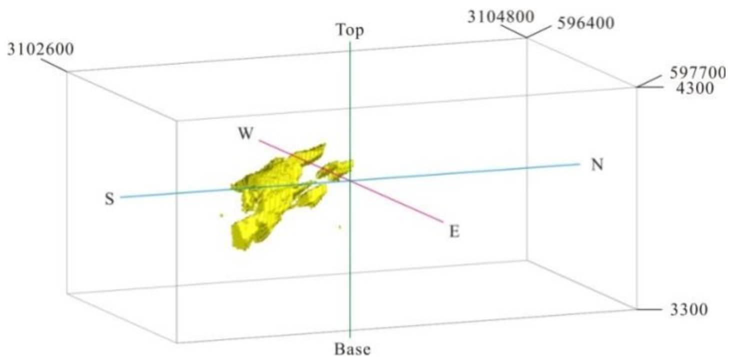
3102600
Top
3104800
596400
597700
4300
W
N
S
E
3300
Base

(c)

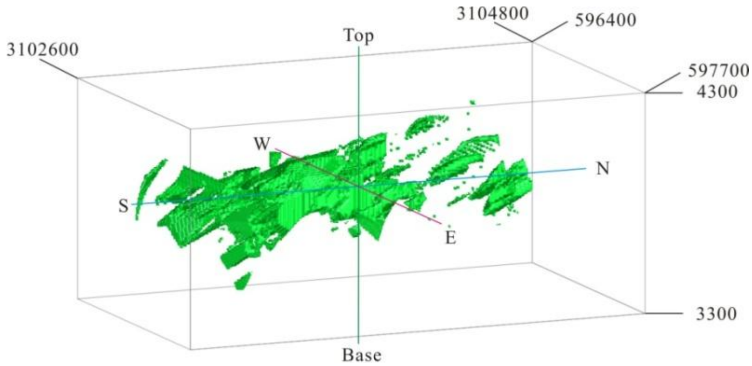
3102600
Top
3104800
596400
597700
4300
W
N
S
E
3300
Base

Fig. 13.

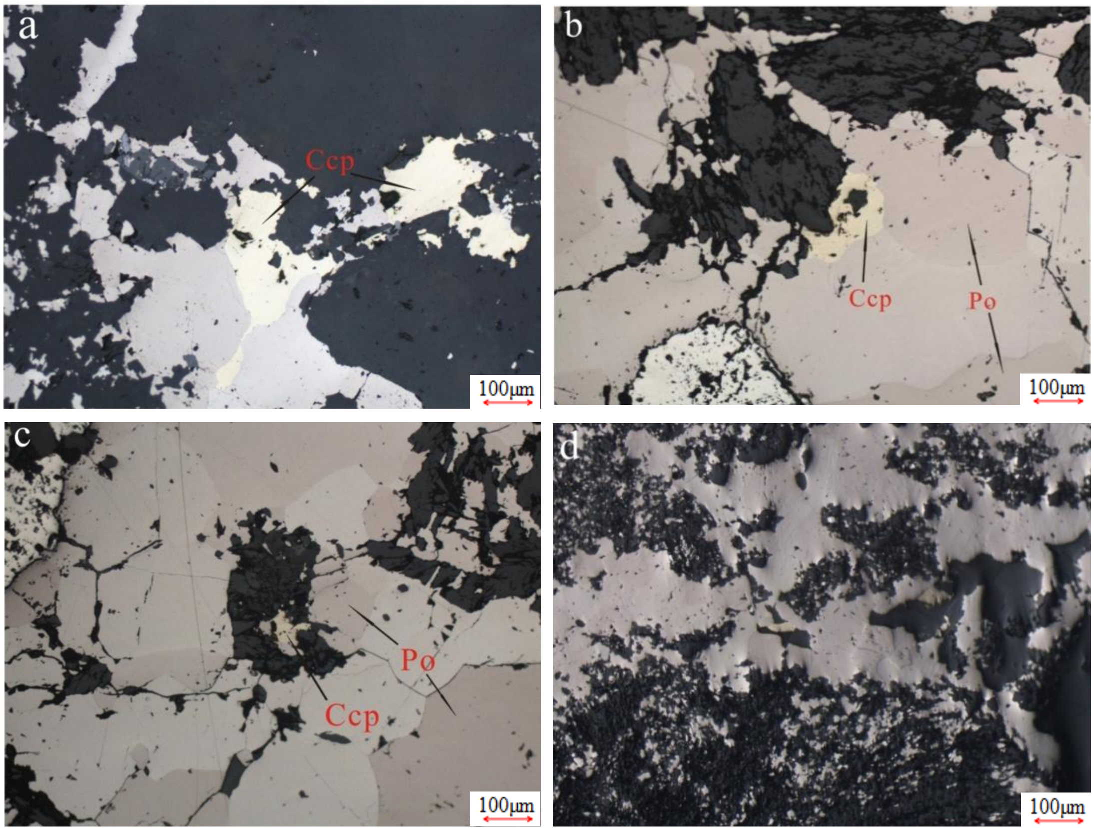

Fig. 14.

Table 1

Variables	Residual
Mean	0.000
Variance	0.016
Standard Deviation	0.127

Table 2

Mineralized zones	Thresholds(Cu%)	Range(Cu%)
Barren host rock		<0.25
Weakly mineralized	0.25	0.25–1.38
Moderately mineralized	1.38	1.38–1.88
Highly mineralized	1.88	>1.88

Table 3

Mineralized zones	PS threshold	Range of PS	Range(Cu%)
leached zone and barren host rock		<7.81	<0.23
hypogene zones	7.81	7.81-8.70	0.23-1.33
supergene enrichment zones	8.70	>8.70	>1.33

Table 4

		Geological model Inside zone	Outside zone
Fractal model	Inside zone	True positive (A)	False positive (B)
	Outside zone	False negative (C)	True negative (D)
		TypeIerror=C/(A+C)	TypeIIerror=B/(B+D)
		Overallaccuracy=(A+D)/(A+B+C+D)	

Table 5

		Potassic alteration of geological model Inside zones	 Outside zones
C–V fractal model of highly mineralized zones	Inside zones Outside zones	A 2850 C 77927 T1E 0.96 OA	B 1360 D 76913 T2E 0.02 0.50
S–V fractal model of supergene enrichment zones	Inside zones Outside zones	A 4131 C 73985 T1E 0.95 OA	B 2318 D 74726 T2E 0.03 0.52

Table 6

		Phyllic alteration of geological model Inside zones	 Outside zones
C–V fractal model of moderately and weakly mineralized zones	Inside zones Outside zones	A 36518 C 25461 T1E 0.41 OA	B 48027 D 69155 T2E 0.40 0.59
S–V fractal model of the hypogene zones	Inside zones Outside zones	A 40080 C 26899 T1E 0.40 OA	B 44943 D 54239 T2E 0.45 0.56

Table 7

Sample no.	Mineralized zones obtained by fractal models	Cu(%)
PL-B74	Weakly mineralized zones	0.41
PL-B62	Moderately mineralized zones	1.32
PL-B82	Highly mineralized zones	1.80